DOI: 10.31401/WS.2023.proc.17



# Penetration of Energetic Electrons from Outer Radiation Belt to Lover L-Values and to Inner Radiation Belt

*Dachev T.P.[1], Tomov B.T.[1], Matviichuk Y.N.[1], Dimitrov P.G.[1], Semkova J.V.[1], Koleva R.T.[1], Jordanova M.M.[1], Bankov N.G.[1], Mitev M.G.[1], Krastev K.N.[1], Malchev S.P.[1], Reitz G.[2], Header D.-P.[3]*

[1]Space Research and Technology Institute, Bulgarian Academy of Sciences, Sofia, Bulgaria
tdachev59@gmail.com
[2]German Aerospace Center (DLR), Institute of Aerospace Medicine, Cologne, Germany
[3]Möhrendorf, Germany

## Abstract

The radiation risk radiometer-dosimeter (R3D)-R2 instrument was situated outside the Russian segment of the International Space Station (ISS) and inside the ESA EXPOSE-R2 facility in the period November 2014 - January 2016. We detected a penetration of the relativistic electrons below L=2.5 in the recovery phase of the magnetic storm after 18 March 2015. In the period March 18-28 2015, the lower boundary of L=1.8 was reached. The relativistic electrons at low L disappeared on March 28, 2015. The magnetic storm on 25th of June 2015 again generated relativistic electrons' fluxes from the Outer Radiation Belt (ORB) at the L values below 2.5. The ORB enhancement on July 4 2015 emphasized them again. In this specific case, the minimal L values reached L=1.6. Almost all disturbances in the Disturbance Storm Time (Dst) index from July 11th, 2015 until January 1st, 2016 generated new portions of relativistic electrons in the L-values below 2.5. They existed for few days and disappeared until the next Dst disturbance.

**Keywords:** outer radiation belt; inner radiation belt; ISS.

## Introduction

High-energy charged particles are trapped by the Earth's magnetic field and form two distinct belts of toroidal shapes surrounding the Earth: the Inner Radiation Belt (IRB) and the Outer Radiation Belt (ORB).

The IRB is situated at an altitude from 0.2 to 2.0 Earth radii at the geomagnetic equator and consists of electrons, with energies of up to 10 MeV, and protons with energies of up to 700 MeV. Outside of the ISS, the IRB energetic protons deliver a daily dose of 567-μGy $d^{-1}$ [Dachev et. al., 2017].

The ORB is located in the altitudinal range from 3.4 to 10 Earth radii. The ORB energetic population is electrons with energies of a few MeV. The first observations of the ORB relativistic electron fluxes in the ISS, on the American laboratory module, were made in 2001 with a Liulin-E094 instrument [Dachev et al., 2002], [Reitz et al., 2005]. Later, the ORB relativistic electron fluxes were observed with more Liulin-type instruments flown on the ISS and LEO satellites [Dachev et al., 2009, 2015], [Dachev, et al., 2015a]. The average daily dose during the entire ESA EXPOSE-R2 mission from the ORB daily dose rate is 278-μGy $d^{-1}$. On quiet days, the ORB daily dose rates is practically zero but reached maximum dose rates up to 3,000-μGy $d^{-1}$ in the disturbed periods after magnetic storms. The most extreme hourly dose rates values that we have registered were 28,840 μGy $h^{-1}$[Dachev et. al., 2017].

## Materials and methods

R3DR2 instrument is a low mass (0.17 kg) and small-dimension (76×76×36 mm) Liulin type spectrometer (LTS) [Dachev et al., 2015a, 2017]. It measures solar UV and visible radiation in four channels and cosmic ionizing radiation in 256 channels respectively. Figure 1 shows the mounting position of the R3DR2 instrument (in red rectangle) in the EXPOSE-R2 facility.

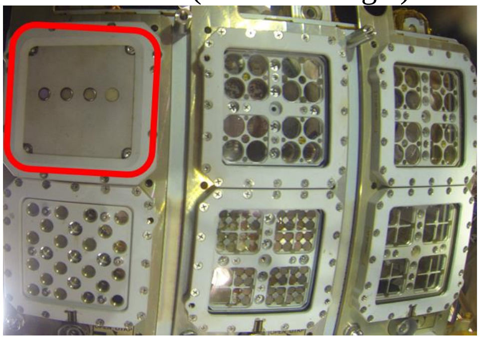

***Figure 1.*** *External view of R3DER2 instrument (in the red rectangle) mounted on EXPOSE-R2 facility. (Picture taken by Russian cosmonaut Alexander Samokutyaev on October 22nd, 2014 during EVA-2 for mounting of EXPOSE-R2 facility outside Russian "Zvezda" module. (Picture credit of ESA/NASA/RKA)*

The doses (deposited energies) are determined in the R3DR2 instrument by Hamamatsu S2744–08 silicon PIN photodiode. The pulse amplitudes from ionized particles, gamma quanta and indirectly neutrons, first pass the charge-sensitive preamplifier then a 12-bit fast analogue-to-digital (A/D) converter, which digitizes them. The pulse amplitudes are proportional by a factor of 240 mV/MeV according to the AMPTEK A225F charge-sensitive preamplifier specifications. The energy loss in the detector and respectively the dose are transformed into digital signals and sorted into 256 channels by a multichannel analyzer. For every exposure interval of 10 s, a single 256 channels energy deposition spectrum is collected.

A system international (SI) determination of the dose is used to calculate the absorbed dose in the silicon detector. The dose in SI is the energy in Joules deposited in one kilogram of matter. The dose *D* (Gy) in the silicon detector is calculated from the spectrum as:

$$D=K* \Sigma_1^{256}(Ei * Ai)/MD, \quad (1)$$

Where *MD* is the mass of the detector (in kg), *Ei* is the energy loss (in Joules) in the channel *i*, *Ai* is the number of events in it, and *K* is a coefficient. Dachev et al. [2002, 2017] have published more details of the dose calculation procedures. According to the formula (1) the dose rate is a function of the count rate in the 256 channels or totally a function of the flux. That is why in the paper these two parameters are interchangeable.

The R3DR2 data selection procedures [Dachev 2009; Dachev et al., 2017] recognize in the near Earth space the following four primary radiation sources: (1) The globally distributed primary Galactic Cosmic Rays (GCR) particles and their secondary products; (2) The inner radiation belt (IRB) trapped protons in the region of the South Atlantic Anomaly (SAA); (3) The relativistic electrons and/or bremsstrahlung in the high latitudes of the station orbits, where the horns of the outer radiation belt (ORB) are situated; (4) The solar energetic particles (SEP). These four radiation sources were measured in the R3DR2 instrument ISS data [Dachev et al., 2016], too.

**Results**

Figure 2 presents the results. Panel (2a) shows the variations of the calculated daily average ORB dose rate from 24 October 2015 until 16 January 2016. Panel (2b) depicts the 3D L and time graphic of the inner and outer belt maximal flux variations. In the top part of panel 2b with black line are the Dst index variations, while the average altitude of ISS (in km) is presented on the bottom.

The simultaneously analysis of the red curve in Panel (2a) and the black curve in Panel (2b) shows that the average daily dose rate anticorrelate the daily Dst index. This is connected with the geomagnetic activity, represented with the Dst index (http://wdc.kugi.kyoto-u.ac.jp/index.html) or solar wind variations. During the quiet time, between October 24, 2014 and the middle of March 2015, the doses delivered by the relativistic electron flux in the ORB are at very low levels - up to 260 μGy d$^{-1}$. Relativistic electron flux typically decreases, by two or three orders of magnitude, during the main phase of geomagnetic storms and recovers to or increases beyond the pre-storm level during the recovery phase, within several days [Zheng et al., 2006].

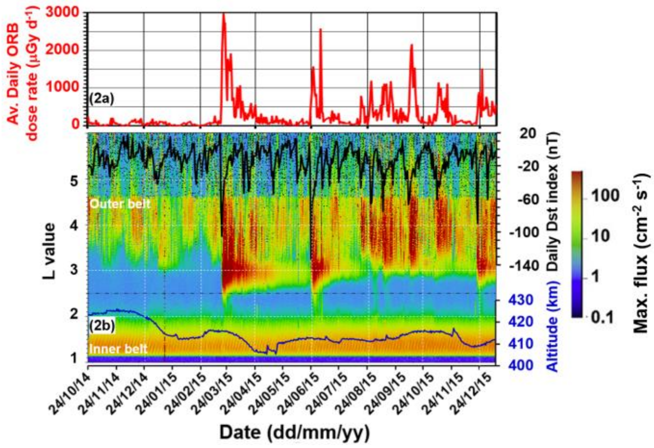


***Figure 2.*** *Panel (2a) presents the Variations of the calculated daily average ORB dose rate from 24 October 2015 until 16 January 2016 as measured by the R3DR2 instrument. Panel (2b) shows 3D L and time graphic of the inner and outer belt maximal fluxes in same range for both belts between 0.1 and 4000 cm$^{-2}$ s$^{-1}$ as seen by the color code bar in the left hand side of the figure. The bins with size of 0.02 L value units are organized in a 442 daily vertical bars. They extend between L equal to two and six against the horizontal date axes. The ISS maximal flux bins cover the whole L values range from 2 to 6 in the Southern hemisphere, while in the Northern hemisphere the flux data bins are extended only up to L = 4.7, due to the asymmetries of the Earth magnetic field. This explains the borderline seen in Fig. 2 at L about 4.7 and the smaller population of the bins in the L range between 4.7 and 6.*

Panel 2b shows both belts. The IRB is distributed in the L range between L=1.2 and L=2.5. This feature is clearly seen in the four upper panels of Figure 3. The IRB maximal dose rate values reached 2500 μGy h$^{-1}$. The flux and dose rate were large during the interval from October to December of 2014; then, they fell until the end of June 2015 and increased again until the end of the measurements. These long-term variations correlated well with the variations in the average altitude of the station (blue line in the bottom of the Panel (2b). The altitudinal dependence in the bottom part of the IRB was studied by the R3DR data [Dachev et al., 2015].

Obvious depletions in the IRB flux, the daily and hourly maximal doses, were observed in the recovery phase of the magnetic storms presented with the Dst curve in Figure 2. We assume that the effect is similar to the one described by [Dachev et al., 2018].

The ORB in Panel (2b) of Figure 2 extends in the L range between 2.5 and 6. The ORB dynamics is much larger than the IRB belt dynamics in both categories maximal flux value and L-value extension.

Two periods are clearly seen in Figure 2 data. In the relatively "quiet" period, the ORB fluxes are relatively small and the equatorward boundary of the ORB varies in the interval of L between 3 and 4. The ORB relativistic electrons equatorward boundary never penetrates at L values below 2.5.

During the "disturbed" period, between 17 March 2015 and the end of the observations, strong variations in the ORB maximal flux and daily average dose rates were observed. The highest maxima was recorded on March 20th 2015, when the daily average dose rate was 2962 $\mu Gy\ d^{-1}$ and the averaged for the day flux was 361 $cm^{-2}\ s^{-1}$.

The penetration of the energetic electrons from outer radiation belt to lover L-values and to inner radiation belt in Figure 2 is seen as yellow-green veils, which extended from the equatorward boundary of ORB down to IRB. The equatorward boundaries of the penetrations are not clear seen. Figure 3 clarifies the penetration dynamics in time and L-value.

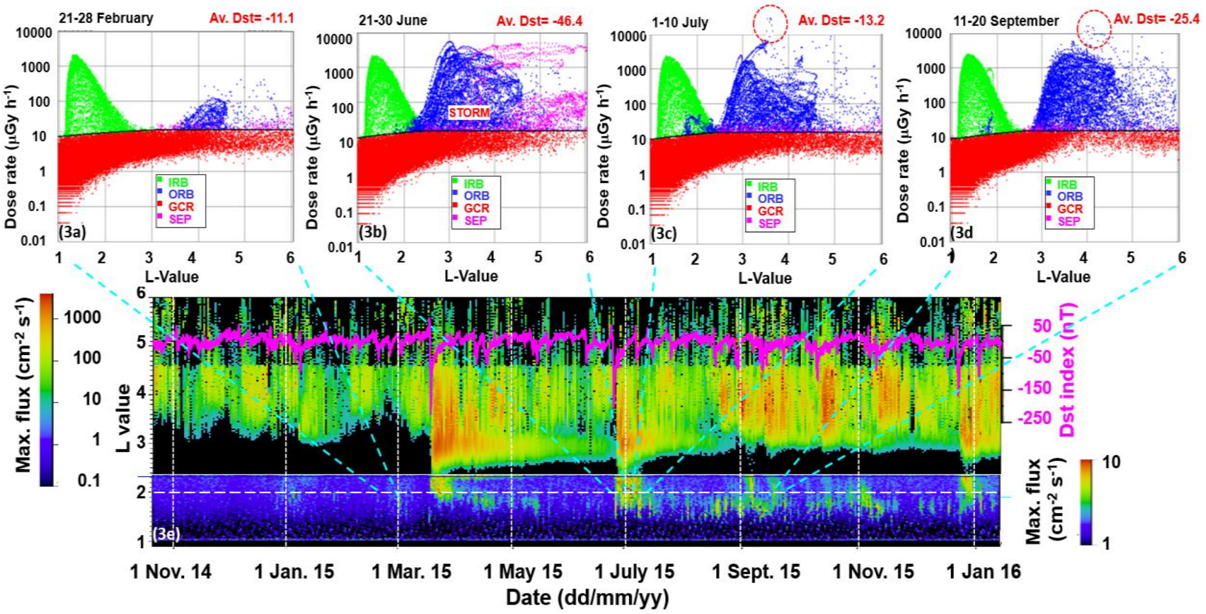


***Figure 3.*** *The upper row with four Panels (3a) to (3d) illustrates the different cases of penetration of energetic electrons toward lower L-values and the inner radiation belt. The Panel (3c) contains two 3D L and time graphics with different maximal flux ranges. Panel (3e) aim is to show the penetration dynamics in time and L-value as seen by the two color code bars in the right and left side of the panels.*

Panel (3a) presents the latitudinal distribution of the dose rates against McIlwain's L values [McIlwain, 1961]. The L value is plotted on the x-axis. On the y-axis, the absorbed dose rate is plotted. Panel (3a) plots 69,312 points with 10-s resolution for 8 days from 21 to 28 February 2015.

Four different primary radiation sources separated by the heavy black line are seen in the data. These sources are plotted in Panel (3a) with four different colors: for the IRB-green, ORB-blue, GCR-red, and SEP-magenta. SEP data represent except the real solar energetic particles a small amount of secondary particles, which are characterized with similar than SEP requirements. From one 10 s independent measurement of the dose rate (D) and flux (F), we were able to calculate one dose to flux ratio (D/F). Using this, we were able to decide only what the predominant radiation sources is, but we are unable to extract the exact doses of each source [Dachev et al., 2017].

Panel (3a) illustrates the sources distribution during one of the quietest geomagnetic periods of the R3DR2 data. The average for 8 days Dst value is -11.1 nT. In these days the maximal ORB source value is at the level of about 220-$\mu Gy\ h^{-1}$, which is the smallest in comparison with other three panels in the first row of Figure 3. In addition, the slot region is the largest and practically empty from any particles. No energetic electrons from the IRB source are observed.

Completely different sources distribution is shown on Panel (3b). The latter presents data for the period 21-30 June 2015 when a geomagnetic storm with a minimal Dst index of -204 nT on 23 June 2015 at 04 UT occurred (http://wdc.kugi.kyoto-u.ac.jp/index.html). GCR and IRB sources do not show any drastic changes in comparison with the data in Panel (3a). The SEP source variations during this period are described in [Dachev et al., 2016], while the IRB source variations in [Dachev et al., 2018].

The ORB dose rate values variations are also well-studied [Dachev et al. 2017] that is why here we will concentrate on ORB spatial variations in L coordinates. The first difference from Panel (3a) seen in Panel (3b) is that the ORB electrons fulfil the whole slot region and extend down to L=1.7 inside the inner belt. Lucking in Panel (3e) we can see that similar process is observed after the main phase of the storm in March 2015. It happens at every Dst disturbance after 18$^{th}$ March 2015. The penetrated electrons patches in low L-value exist for a few days, disappear and appear again at next geomagnetic disturbance.

Second difference in Panel (3b) is the existence of two large profiles in L-value of SEP particles (magenta points), generated after the SEP event that started on 21 of June 2015 at 21:35 UT (https://umbra.nascom.nasa.gov/SEP/). The smaller SEP dose rate values profile reflects the values in the end of SEP event, while the larger the doses - the beginning [Dachev et al., 2016].

Panel (3c) presents the most dynamic 10 days ORB source distribution in L-values for the whole period of observations between November 2014 and January 2016. High dose rate patches are seen. The largest penetration of relativistic electrons below L=2 is observed. Also, in the dashed line oval in the top part of the panel are seen points with dose rate values larger than 10,000-μGy $h^{-1}$, which according to our classification in [Dachev et al., 2018] are indications of "Precipitation bands" [Blake et al., 1996]. The maximum ORB ever observed flux for 10-s of 11,813 $cm^{-2}$ $s^{-1}$ and dose rate of 28,840 μGy $h^{-1}$ values were observed at about 22:30 local magnetic time on 4$^{th}$ of July 2015. The average daily dose rate maximum on the 4$^{th}$ of July is the second largest in Panel (3a) of Figure 3

Panel (3d) is remarkable that even that the slot region is empty of ORB energetic electrons in the L-value range 1.6-2 they energetic electrons still exists.

The Panel (3e) contains two 3D L and time graphics with different maximal flux ranges as seen by the two color code bars in the right and left side of the Panel. The lover part of the Panel (3e) in the L range from 1.2 to 2.4 presents the whole dynamics of the penetrations of relativistic electrons between 24 October 2014 and 16 January 2016.

Similarly to [Claudepierre et al. 2017], we recorded the first strong penetration of the relativistic electrons below L=2.5 on March 18, 2015. In the period March 18–28, 2015 the lowest boundary of L=1.7 was reached. Then the relativistic electrons at a low L disappeared on March 28, 2015. The storm on June 25, 2015 moved again the fluxes of ORB relativistic electrons at L-values below two and they are clearly seen in the lower part of Panel (3e). The ORB enhancement on July 4, 2015 emphasized them again but at this case the minimal L-values reached was L=1.6. Almost all disturbances in the Dst from July 11, 2015 until January 1, 2016 generated a new portion of relativistic electrons in the range of L-values between 1.6 and 2. They existed for few days and disappeared until the next Dst disturbance and magnetic substorm.

## Conclusions

The most important achievement of the paper is the discovery and the proof of the existence of the relativistic electron fluxes (REF) in the R3DR2 data in the slot region and inner radiation belt in the time after the magnetic storms in March and June 2015;

All REF were observed in the period March-December 2015 during the EXPOSE-R2 mission. REF were not observed in the slot region and inner radiation belt during EXPOSE-E and EXPOSE-R missions. Never the less that, relativistic electrons fluxes do not pose a real health concerns for astronauts being on extravehicular activities it is important this phenomena to be further studied.

**Acknowledgements**

The authors would like to thank all Bulgarian and foreign specialists and organizations that participated in the development and funding of the projects with Liulin equipment. The authors would like to express their deepest gratitude to the astronauts and cosmonauts aboard the manned space stations "Mir" and ISS for conducting experiments with Liulin spectrometers.

**Data availability**

The data, used in this paper, are part of the "Unified web-based database with Liulin-type instruments" that are available online, free of charge at the following URL: http://esa-pro.space.bas.bg/database. The database contains data from nine Liulin type experiments around the Earth and Liulin-MO data in the path to Mars (2016-2017) and in Mars orbit (Since 2017) [Semkova et al., 2023]. Each data point contains up to 256 parameters, which except the measured values listed the time and space parameters of the carrier.

**References**

Blake, J.B., Looper, M.D., Baker, D.N., Nakamura, R., Klecker, B., Hovestadt, D., 1996. New high temporal and spatial resolution measurements by SAMPEX of the precipitation of relativistic electrons. Adv. Space Res. 18 (8), 171–186.

Claudepierre, S.G., et al. 2017. The hidden dynamics of relativistic electrons (0.7-1.5 MeV) in the inner zone and slot region. J. Geophys. Res. Space Physics 122. https://doi.org/10.1002/2016JA023719.

Dachev, T., Tomov, B., Matviichuk, Y., Dimitrov, P., Lemaire, J., Gregoire, G., Spurny, F., 2002. Calibration results obtained with Liulin-4 type dosimeters. Adv. Space Res. 30, 917–925. https://doi.org/10.1016/S0273-1177(02)00411-8.

Dachev, T.P., 2009. Characterization of near Earth radiation environment by Liulin type instruments. Adv. Space Res. 44, 1441–1449. https://doi.org/10.1016/j.asr.2009.08.007.

Dachev, T.P., Tomov, B.T., Matviichuk, Yu.N., Dimitrov, Pl.G., Bankov, N.G., Shurshakov, V.V., Ivanova, O.A., Hader, D.-.P., Schuster, M.T., Reitz, G., Horneck, G., 2015. "BION-M" №1 spacecraft radiation environment as observed by the RD3-B3 radiometer-dosimeter in April-May 2013. Journal of Atmospheric and Solar-Terrestrial Physics 123, 82–91. https://doi.org/10.1016/j.jastp.2014.12.011.

Dachev, T.P., Semkova, J.V., Tomov, B.T., Matviichuk, Y.N., Dimitrov, P.G., Koleva, R.T., Kubancak, I.N., 2015a. Overview of the Liulin type instruments for space radiation measurement and their scientific results. Life Sci. Space Res. 4, 92–114. https://doi.org/10.1016/j.lssr.2015.01.005.

Dachev, T.P., Tomov, B.T., Matviichuk, Y.N., Dimitrov, P.G., Bankov, N.G., 2016. High dose rates obtained outside ISS in June 2015 during SEP event. Life Sci. Space Res. 9, 84–92. https://doi.org/10.1016/j.lssr.2016.03.004.

Dachev, T.P., Bankov, N.G., Tomov, B.T., Matviichuk, Y.N., Dimitrov, P.G., Häder, D.-P, Horneck, G., 2017. Overview of the ISS radiation environment observed during the ESA EXPOSE-R2 mission in 2014–2016. Space Weather, Vol. 15, 1475–1489, https://doi.org/10.1002/2016SW001580.

Dachev, T.P., South-Atlantic Anomaly Magnetic Storms Effects as Observed outside the International Space Station in 2008-2016, 2018. JASTP, 179, 251-260. https://doi.org/10.1016/j.jastp.2018.08.009

McIlwain, C.E. (1961). Coordinates for mapping the distribution of magnetically trapped particles. Journal of Geophysical Research, 66, 3681–3691. https://doi.org/10.1029/JZ066i011p03681

Reitz, G., Beaujean, R., Benton, E., Burmeister, S., Dachev, T., Deme, S., Olko, P., 2005. Space radiation measurements on-board ISS-the DOSMAP experiment. Radiat Dosimetry 116, 374–379. https://doi.org/10.1093/rpd/nci262.

Semkova, J., Koleva, R., Benghin, V., Krastev, K., Matviichuk, Y., Tomov, B., Maltchev, S., Dachev, T., Bankov, N., Mitrofanov, I. and Malakhov, A., 2023. Observation of the radiation environment and solar energetic particle events in Mars orbit in May 2018-June 2022. Life Sciences in Space Research. https://doi.org/10.1016/j.lssr.2023.03.006.

Zheng, Y., Lui, A.T.Y., Li, X., Fok, M.-C., 2006. Characteristics of 2–6 MeV electrons in the slot region and inner radiation belt. J. Geophys. Res. 111, A10204. https://doi.org/10.1029/2006JA011748.